

# Optical constants of germanium and thermally grown germanium dioxide from 0.5 to 6.6 eV via a multisample ellipsometry investigation

Timothy Nathan Nunley, Nalin S. Fernando, Nuwanjula Samarasingha, Jaime M. Moya, Cayla M. Nelson, Amber A. Medina, and Stefan Zollner<sup>a)</sup>

Department of Physics, New Mexico State University, MSC 3D, P.O. Box 30001, Las Cruces, New Mexico 88003-8001

(Received 22 May 2016; accepted 7 September 2016; published 30 September 2016)

Thermal GeO<sub>2</sub> oxides up to 136 nm thickness were produced by annealing Ge wafers in pure oxygen at 550 °C and 270 kPa pressure for up to 10 h. The oxidation kinetics followed the Deal–Grove law. Using multisample spectroscopic ellipsometry for a series of five thermal oxides with different thicknesses, the complex dielectric functions of Ge and GeO<sub>2</sub> were determined from 0.5 to 6.6 eV, for thin-film metrology applications in Ge-based microelectronics and photonics. The dispersion of the GeO<sub>2</sub> layer was modeled with a simple Tauc-Lorentz oscillator model, but a more complicated dispersion with eight parametric oscillators was required for Ge. A reasonable fit to the ellipsometric angles could be obtained by assuming that all thermal oxides can be described by the same dielectric function, regardless of thickness, but a slight improvement was achieved by allowing for a lower density oxide near the surface of the thickest films. The authors compare their results with literature data for Ge and bulk and thin-film GeO<sub>2</sub>. © 2016 American Vacuum Society. [<http://dx.doi.org/10.1116/1.4963075>]

## I. INTRODUCTION

Optical constants (complex refractive index  $n$ , complex dielectric function  $\epsilon$ , and reflection and absorption coefficients  $R$  and  $\alpha$ ) of materials are of great importance for optical metrology in the semiconductor industry.<sup>1,2</sup> A high-performance complementary-metal-oxide-semiconductor process flow with 11 layers of metal requires about 75 photolayers and may contain up to 100 thickness measurements, most of them performed using spectroscopic ellipsometry.<sup>3</sup> This technique has been described in various books with increasing levels of sophistication.<sup>4–7</sup>

Since most microelectronic devices are built on a Si wafer, the optical constants of Si and SiO<sub>2</sub> are the most important ones and have been determined with greater accuracy than other materials.<sup>8</sup> They are often referred to as *Woollam silicon* and used almost universally for thickness measurements in factories around the world. For many materials, optical constants have been tabulated by Palik<sup>9</sup> and Adachi.<sup>10</sup> Optical constants of intrinsic materials are related to their vibrational and electronic properties.<sup>11–15</sup>

Optical constants are determined using different techniques: below<sup>16</sup> or near<sup>17,18</sup> the band gap of a semiconductor, the absorption coefficient  $\alpha$  and refractive index  $n$  are determined using transmission and minimum-deviation prism<sup>19</sup> measurements, respectively. These techniques (and data resulting from them) are still the most useful today and have not been replaced by more modern methods, such as spectroscopic ellipsometry, which is not suitable for measuring small absorption coefficients below about 10<sup>3</sup> cm<sup>-1</sup> (see Refs. 20 and 21). Above the band gap, transmission measurements on thin films can be successful.<sup>22</sup> Since about 1960, the complex dielectric function above the band gap has been determined by reflectance followed by Kramers–Kronig transformation,<sup>23</sup> but such

results are often plagued by systematic errors due to surface overlayers (including surface roughness) and the limited spectral range of the measurement.

More recently, the optical constants of semiconductors have been determined by spectroscopic ellipsometry. Early instrument designs suffered from the rotating-analyzer artifact<sup>24,25</sup> and could not measure small absorption coefficients accurately. This accuracy was improved by instruments employing a polarization modulator<sup>26</sup> or a computer-controller Berek waveplate compensator.<sup>8</sup> Even the most precise spectroscopic ellipsometers are unable to compete with transmission or minimum-deviation prism measurements to determine the optical constants below the band gap. We note that transmission measurements must be performed using two-side polished wafers, while ellipsometry measurements are better taken on single-side polished wafers, because reflections from a polished (or insufficiently roughened) back surface interact incoherently with the reflection from the front surface, thus causing depolarization of the reflected light beam.<sup>5</sup>

Ellipsometry measurements on bulk semiconductors are difficult to interpret because semiconductor wafers are usually covered by native oxides and have a slightly rough surface. Modeling ellipsometry data from a real semiconductor surface requires precise knowledge of the optical constants of the substrate (for example, Ge), the surface layer (native oxide and roughness), and the thickness of the surface layer. There are too many unknowns in the model to determine all of them in measurements of a single sample.

Aspnes and Studna<sup>24</sup> addressed this problem for Ge by minimizing the surface layer thickness with wet chemical etching (using a bromine solution in methanol, buffered hydrofluoric acid, followed by a water rinse) and thus optimizing the height of the absorption near the  $E_2$  critical point at 4.26 eV. They achieved an  $\langle\epsilon_2\rangle$  peak value of 30.6 at 4.26 eV, which is still only a lower bound for the true value of

<sup>a)</sup>Electronic mail: [zollner@nmsu.edu](mailto:zollner@nmsu.edu); URL: <http://ellipsometry.nmsu.edu>

$\epsilon_2$  for Ge at this energy because it was not corrected for the oxide or roughness layer. Cleaving a bulk Ge crystal in ultra-high vacuum<sup>27</sup> or cleaning the surface through ion bombardment<sup>28</sup> followed by annealing to produce clean  $2 \times 8$  or  $2 \times 1$  reconstructed surfaces also introduces uncertainties because of the distortion of the polarization state by windows<sup>5</sup> and because of surface roughness, ion bombardment damage, and epi-optical effects, which make the optical constants dependent on surface orientation<sup>29</sup> or surface passivation.

A different approach was taken by Jellison,<sup>26</sup> whose intent of wafer cleaning was to remove carbon-based surface contamination (with acetone, methanol, and peroxide, followed by a water rinse), but not the surface oxide itself. The thickness of the remaining stable native oxide was then determined with an ellipsometric measurement slightly above the direct band gap, where the absorption of Ge is small. This is known as the Jellison–Sales method for transparent glasses.<sup>30</sup> It works well, if the optical constants of the surface overlayer are known precisely, but fails otherwise. Jellison found an  $\epsilon_2$  peak value of 31.8 at 4.24 eV, slightly higher than the result from Aspnes and Studna<sup>24</sup> because of the native oxide layer correction.

Finally, Herzinger *et al.*<sup>8</sup> described a method to determine the optical constants of semiconductors, if the optical constants of the substrate, those of the oxide overlayer, and the layer thickness are all unknown. This method requires a series of samples consisting of the same substrate and the same oxide, where only the oxide thickness is varied. Ellipsometry measurements of several such samples with oxide thicknesses ranging from very thin (only native oxide) to as thick as possible (limited by the rate of oxidation) yield the optical constants of the substrate, those of the oxide, and the thicknesses of all layers. The only assumption used by this method is that the optical constants of the oxide do not vary with thickness (or from one sample to another). The validity of this assumption can be checked by inspecting the goodness of fit for all samples.

This method has only been used for Si so far,<sup>8</sup> where uniform and repeatable thermal oxides with arbitrary thicknesses are easily produced with well established silicon manufacturing techniques.<sup>31</sup> It has led to universally accepted values for the optical constants of Si (100) and its thermal oxide.<sup>8</sup> The purpose of this paper is to use the same method to determine the optical constants of bulk Ge with a (100) surface orientation and those of thermally grown GeO<sub>2</sub>. Precise knowledge of Ge optical constants is important for the development of Ge-based p-type metal-oxide-semiconductor devices, which have attracted much attention recently.<sup>32</sup> The optical constants of thin Ge layers may, of course, be different from those of bulk Ge, but that is beyond the scope of this article.

This article is organized as follows: We first describe our experimental methods to clean the Ge substrate, prepare thermal GeO<sub>2</sub> oxides, and ellipsometry data acquisition and analysis. Next, we present our results for GeO<sub>2</sub> on Ge in a three-phase (ambient/oxide/substrate) model, followed by a discussion if this model can be improved by including a thin interfacial layer between the GeO<sub>2</sub> and the substrate or by allowing the GeO<sub>2</sub> refractive index to vary between samples.

Finally, we discuss our overall results and compare our findings to previous data.

## II. THERMAL OXIDATION OF Ge

The as-received Ge bulk wafers were cleaved into  $20 \times 20 \text{ mm}^2$  pieces. These pieces were then subjected to an ozone clean in a Novascan PSD Pro series digital UV ozone system utilizing a Hg vapor lamp. This cleaning was performed in an oxygen-enriched environment, achieved by allowing ultrapure (99.98%) oxygen to flow through the system for several minutes before sealing the chamber with the Hg lamp on and the sample on a heating stage held at 150 °C for 60 min, followed by a 30-min period of incubation with the lamp off and the sample cooling to room temperature. After the ozone clean, samples were cleaned ultrasonically for 20 min in deionized water, followed by 20 min in isopropanol.

The intent of this hybrid dry/wet clean is to remove carbon-containing surface contaminants from the wafer and reduce the native oxide thickness, but leave a thin stable oxide on the wafer<sup>26</sup> as a seed oxide for thermal oxidation. Unlike Ref. 33, we did not use harsh chemicals (bromine or hydrofluoric acid) before oxidation to avoid roughening or contaminating the surface. Some elements used for our cleaning process, especially the use of reactive oxygen species, are similar to those of Ref. 34. Photoemission studies have shown that exposure to UV light leads to a predominance of the Ge<sup>4+</sup> oxidation state.<sup>35</sup>

After cleaning, the samples were placed in an ULVAC-RIKO MILA-5000 infrared lamp heating system for rapid thermal annealing. Samples were annealed in ultrapure oxygen with 170 kPa gauge pressure (270 kPa absolute), as measured by the gas regulator, at 1 l/min flow at 550 °C for several hours, as needed to achieve the desired oxide thickness.<sup>33</sup> Table I lists the annealing times for several samples as well as their thicknesses and other parameters.

GeO<sub>2</sub> is hygroscopic and water soluble.<sup>36</sup> Therefore, ellipsometry measurements were performed within a few days after oxidation. Furthermore, thermal GeO<sub>2</sub> desorbs by reaction with the Ge substrate and diffusion of oxygen vacancies generated at the Ge/GeO<sub>2</sub> interface.<sup>37</sup> Higher

TABLE I. List of GeO<sub>2</sub> oxides produced by thermal oxidation of Ge substrates at 2.7 atm oxygen pressure at 550 °C.  $d$  is the oxide thickness from ellipsometry,  $t$  the oxidation time,  $\Delta d$  the relative thickness nonuniformity determined from the ellipsometry depolarization spectra,  $d_{\text{XRR}}$  the thickness determined by XRR (samples 4 and 5 were fit with a fixed thickness), and  $\langle \rho \rangle$  the electron density determined by XRR. Ellipsometry results are from two models (uniform and graded) as discussed in Sec. IV (MSE = 14) and V (MSE = 6.9). Probable errors are given in parentheses.

No.	$t$ (h)	Uniform			Graded		
		$d$ (nm)	$\Delta d$ (%)	$d$ (nm)	$\Delta d$ (%)	$d_{\text{XRR}}$ (nm)	$\langle \rho \rangle$ (e/Å <sup>3</sup> )
1	0	2.31(1)	NA	2.31(1)	NA	NA	NA
2	1	34.01(3)	8.0(2)	35.32(2)	6.0(1)	33.3	1.03
3	2	52.18(3)	6.0(1)	53.31(2)	6.0(1)	50.2	1.03
4	5	88.62(5)	8.0(2)	92.11(5)	7.0(1)	92.5(f)	1.00
5	10	135.94(6)	1.5(1)	141.69(5)	1.0(1)	142(f)	1.01

oxidation temperatures and lower oxygen pressures promote  $\text{GeO}_2$  desorption. We selected an oxidation temperature of  $550^\circ\text{C}$ , because it allows a suitable thermal oxide growth rate with minimal oxide desorption and lowest interface trap density.<sup>38–40</sup> The oxidation pressure of 2.7 atm also enhances oxidation and suppresses thermal oxide desorption, compared to atmospheric pressure.<sup>36</sup>

The resulting  $\text{GeO}_2/\text{Ge}$  layers were brown, yellow-brown, and light blue in appearance (with increasing thickness), with reasonably uniform thickness and occasional spots. Optimizing the clean was crucial to the success of our annealing experiments. We found that thermal oxidation (see Table II and Fig. 1) follows the Deal–Grove model<sup>31</sup>

$$d^2 + Ad = B(t + \tau), \quad (1)$$

where  $d$  is the oxide thickness (determined from ellipsometry as described below),  $t$  the oxidation time, and  $A$ ,  $B$ , and  $\tau$  are parameters that depend on the oxidation conditions, such as temperature, pressure, and gas composition. As shown by the dashed lines in Fig. 1, the oxide thickness depends nearly quadratically on oxidation time, i.e.,  $d^2 \approx B(t + \tau)$ . Including the linear term  $Ad$  (solid line) becomes important for thinner oxides and higher pressures. The oxidation is much faster at higher pressure.

We characterized our layers using grazing-incidence x-ray reflectance (XRR) as shown in Fig. 2. These XRR spectra show a double critical angle for the Ge substrate ( $1.35 \text{ e}/\text{\AA}^3$  density) and the  $\text{GeO}_2$  layer with a lower density ( $1.03 \text{ e}/\text{\AA}^3$ ). The interference fringes (if present) indicate uniform oxide layers with a well-defined electron density. We could only find such fringes for the thinner oxide layers, where XRR thickness and ellipsometry thickness agree to be within 1 nm (which could be explained with surface roughness). From fitting the XRR spectra for thinner oxides, we are able to determine the electron density as a function of depth, also shown in Fig. 2. Thicker oxide layers do not

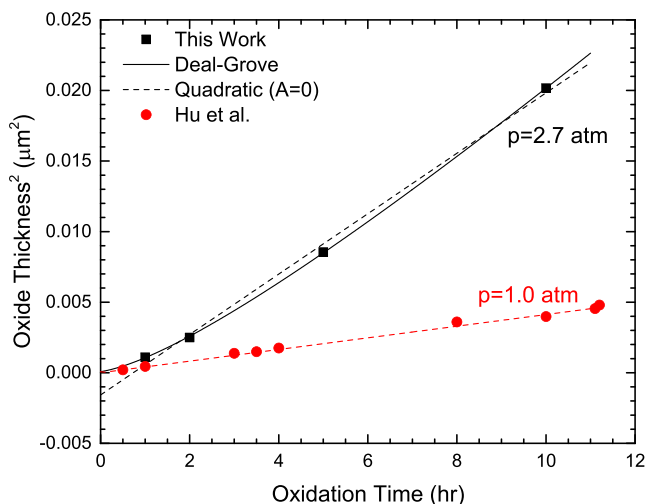


Fig. 1. (Color online) Thermal oxide thickness vs oxidation time at atmospheric pressure (Ref. 33) and at 2.7 atm (this work). The solid line shows the best fit to Eq. (1), while the dashed lines assume a quadratic dependence of the thickness on oxidation time ( $A=0$ ).

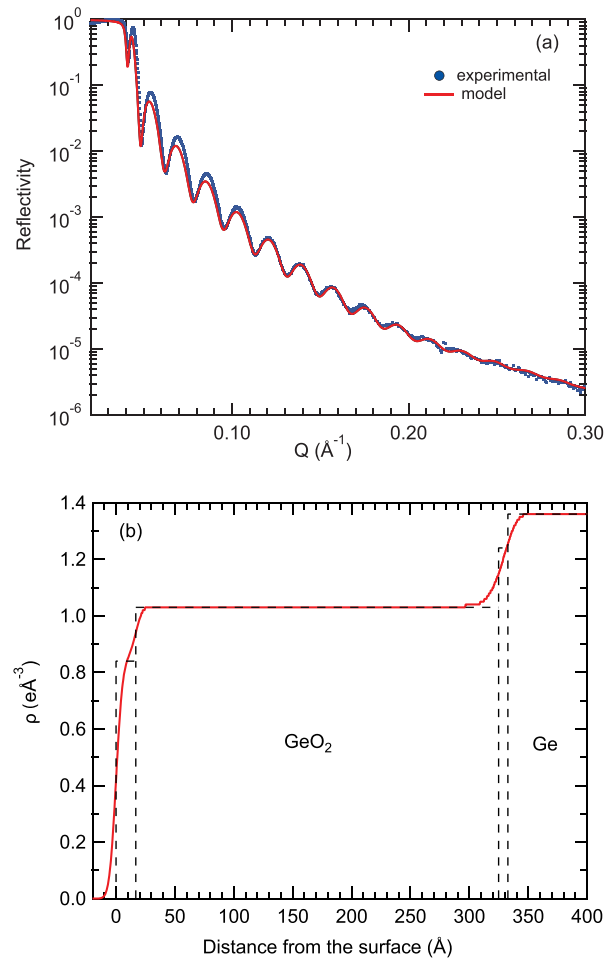


Fig. 2. (Color online) (a) Grazing-incidence x-ray reflectance spectrum (line: model; ●: data) and (b) electron density vs depth for sample 2 (33 nm thickness).

show interference fringes, perhaps due to thickness nonuniformity or a density gradient in the oxide.

Symmetric  $\omega$ - $2\theta$  powder x-ray diffraction scans on a sealed-tube instrument with 1.8 kW power are similar for all samples and only show background and the  $2 \times \text{Ge}(002)$  and  $\text{Ge}(004)$  substrate peaks. We did not find the amorphous  $\text{GeO}_2$  diffraction peak at  $2\theta = 25^\circ$  seen on rf sputtered  $\text{GeO}_2$  films,<sup>41</sup> which were up to 100 times thicker than our thermally grown oxides. Unpolarized Raman spectra with 532 nm laser excitation are similar for all of our samples and only show first- and second-order Raman peaks from the Ge substrate and no significant peaks that might be attributed to  $\text{GeO}_2$ . FTIR ellipsometry and transmission results to investigate the infrared active phonons of these oxides will be discussed elsewhere.

### III. ELLIPSOMETRY MEASUREMENTS AND DATA ANALYSIS

We acquired the ellipsometric angles  $\psi$  and  $\Delta$  and the depolarization spectra from 0.5 to 6.6 eV with 0.01 eV steps on a J.A. Woollam vertical variable-angle-of-incidence rotating-analyzer ellipsometer with a computer-controlled Berek waveplate compensator.<sup>42</sup> To reduce experimental errors, all data

TABLE II. Deal–Grove parameters  $A$ ,  $B$ , and  $\tau$  from Eq. (1) for thermal oxidation of Ge in pure O<sub>2</sub> at temperature  $T$  and pressure  $p$ . Probable errors are given in parentheses.

$T$ (°C)	$p$ (kPa)	$A$ (nm)	$B$ (nm <sup>2</sup> /h)	$\tau$ (h)	
550	100	0	432	0	From Ref. 33
550	270	90(37)	3225(440)	0.22(32)	This work

were obtained by averaging two-zone measurements with equal and opposite polarizer angles. Data were acquired for four angles of incidence ( $\phi_0 = 60^\circ$ ,  $65^\circ$ ,  $70^\circ$ , and  $75^\circ$ ). Larger incidence angles would be desirable to have data near the Brewster regime for bulk Ge, but such measurements are not practical because of the finite sample size and nonuniform oxide thickness. The magnitude of the polarizer angle was kept equal to  $\psi$  at each wavelength, but no less than  $5^\circ$ . The time needed to acquire data for one sample was several hours.

Monochromatic light was produced by an HS-190 double monochromator equipped with three sets of gratings for the near-infrared (NIR), visible (VIS), and quartz-ultraviolet (QUV) portion of the spectral range. The linear dispersion of the monochromator is 2.3 nm/mm in the VIS/QUV and 4.6 nm/mm in the NIR, leading to spectral bandwidths of no more than 4 and 8 nm, respectively, for a maximum slit width of 1.7 mm.

For the spectral range from 0.76 to 6.6 eV, we used a UV-enhanced optical fiber and a 75 W Xe short-arc lamp (Hamamatsu L10873) to produce the incident monochromatic beam. We also measured from 0.5 to 3.0 eV using an IR-enhanced optical fiber and a 100 W quartz-tungsten-halogen lamp (Ushio, with a TDK-Lambda ZUP20–20 power supply), also mounted on the HS-190 monochromator using a slightly modified reflector insert capable of holding and powering the tungsten lamp. This IR setup slightly extends the spectral range downward to 0.5 eV and avoids the strong peaks of the Xe lamp and the opaque region of the UV fiber from 0.88 to 0.92 eV. Data obtained with both setups were merged and showed good agreement in the region of spectral overlap. As one might expect, only the Ge wafer with the thinnest (native) oxide layer showed a slightly unstable oxide due to ongoing oxidation.

The ellipsometric angles ( $\psi$  and  $\Delta$ ) and the Fresnel reflectance ratio  $\rho = e^{i\Delta} \tan \psi$  are related to the pseudorefractive index  $\langle n \rangle$  and the pseudodielectric function  $\langle \epsilon \rangle = \langle n \rangle^2$  of the sample through<sup>4,5</sup>

$$\rho = \frac{\langle n \rangle \cos \phi_0 - \cos \phi_1}{\langle n \rangle \cos \phi_0 + \cos \phi_1} \frac{(\cos \phi_0 + \langle n \rangle \cos \phi_1)}{(\cos \phi_0 - \langle n \rangle \cos \phi_1)}, \quad (2)$$

where  $\phi_0$  is the angle of incidence and  $\phi_1$  the angle of refraction. For an ideal sample without surface overlayers,  $\langle n \rangle$  and  $\langle \epsilon \rangle$  are equal to the refractive index  $n$  and the dielectric function  $\epsilon = n^2$ . The ellipsometric angles for a sample consisting of one or more layers on a substrate can be calculated if the optical constants for all materials are known (or assumed to follow a model).<sup>4–7</sup>

The complex dielectric function  $\epsilon$  for an amorphous oxide like thermally grown GeO<sub>2</sub> is usually described by the Tauc–Lorentz model, where the imaginary part of  $\epsilon$  as a function of photon energy  $E$  is given by<sup>5,6,43</sup>

$$\epsilon_2(E) = \frac{AE_0\Gamma(E - E_g)^2}{E[(E^2 - E_0^2)^2 + \Gamma^2E^2]}, \quad (3)$$

for  $E > E_g$  and vanishes below  $E_g$ . The real part is obtained by Kramers–Kronig transform. This model contains the following parameters:  $E_g$  is the Tauc gap, the onset of absorption. The Lorentz oscillator<sup>44</sup> resonance energy is  $E_0$ , its amplitude  $A$ , and its broadening  $\Gamma$ .

In addition, we use two poles<sup>4</sup> (unbroadened Lorentz oscillators)

$$\epsilon(E) = \frac{A}{E_0^2 - E^2} \quad (4)$$

(where the resonance energies are often chosen arbitrarily as 0.01 and 11 eV) to describe the influence of absorption peaks below or above our spectral range on the dispersion. For crystalline, tetragonal (rutile) GeO<sub>2</sub>, the dominant transverse optical phonon modes for the ordinary ( $E_u$ ) and extraordinary ( $A_{2u}$ ) beams have energies of 41 and 65 meV, respectively.<sup>45</sup> Glassy germania<sup>46,47</sup> also has a significantly higher IR absorption band located at 111 meV. An IR pole at 0.05 eV was chosen for our model.

Finding a parametric model for semiconductors like Ge with a finite number of adjustable parameters requires some thought. In principle, the analytical properties of the complex dielectric function imply that it can be written as a product defined by its poles and zeroes in the complex plane, which can be approximated as a sum of Lorentzians. Seven Lorentzians<sup>48</sup> are sufficient to fit  $\epsilon$  for GaAs between 1.5 and 5.0 eV, but more terms are needed outside of this range. More flexibility can be introduced by allowing Lorentzians with a complex amplitude.<sup>44</sup>

A different approach was taken by Aspnes,<sup>49</sup> who calculated the absorption of semiconductors assuming parabolic bands and constant dipole matrix elements. This critical-point parabolic-band model gives a good description of the derivatives of the dielectric function, but fails to describe  $\epsilon$  away from the critical point singularities, where the nonparabolicity and the  $k$ -dependence of the dipole matrix element have to be taken into account.<sup>50</sup>

More general models for  $\epsilon$  can be constructed from the superposition of critical point structures, which are composed of continuous polynomial sections with Gaussian broadening.<sup>8,50,51</sup> The details of such models are complicated and not relevant for our work, but they describe the dispersion of the dielectric function and its derivatives in a Kramers–Kronig-consistent fashion with a reasonable number of parameters (about 40, compared to 1200 values for  $\epsilon$ ). To be specific, we describe  $\epsilon$  for Ge with the Herzinger–Johs parametric oscillator model<sup>51</sup> as implemented in the wvASE32 software package.<sup>42</sup> We also included a UV pole at 11 eV, but no IR pole because IR lattice absorption is weak

for a nonpolar material like Ge.<sup>16</sup> The number of free parameters can be reduced by keeping some of the shape parameters for Ge the same as those chosen previously<sup>51</sup> for GaAs.

Quoting from Ref. 44, “no attempts are made to give a physical meaning to the models.” We use them primarily to achieve a flexible Kramers-Kronig-consistent description of the dispersion of real materials with a manageable number of parameters. In some cases, fit parameters such as energies or broadenings are related to actual materials properties (such as band gaps), but such agreement is often accidental and should not be over-interpreted. Only the dispersion of the complex dielectric function and the layer thicknesses are actual outcomes of our fit, but none of the oscillator parameters in this analysis.

Once the model has been built, one varies the parameters using the Levenberg–Marquardt algorithm to minimize the mean-squared error (MSE)

$$\text{MSE} = \sqrt{\frac{1}{3N - M} \sum_{i=1}^{3N} \left| \frac{\rho_i^{\text{mod}} - \rho_i^{\text{exp}}}{\Delta \rho_i^{\text{exp}}} \right|^2}, \quad (5)$$

where  $N$  is the number of data points (all photon energies, incidence angles, and samples),  $M$  the number of parameters,  $\rho_i^{\text{exp}}$  the three experimental quantities (ellipsometric angles  $\psi$  and  $\Delta$  and depolarization) at each data point,  $\rho_i^{\text{mod}}$  the quantities calculated from the model, and  $\Delta \rho_i^{\text{exp}}$  the experimental errors.

#### IV. RESULTS FOR GeO<sub>2</sub> ON Ge WITH UNIFORM LAYER FITS

The ellipsometric angles and the depolarization for all five Ge/GeO<sub>2</sub> samples were acquired from 0.5 to 6.6 eV as described earlier. This results in ten data sets in the NIR/VIS and VIS/QUV spectral range. All data were loaded into our software and fitted simultaneously.

Figures 3 and 4 show the ellipsometric angles and the pseudodielectric function  $\langle \epsilon \rangle$  for the sample with the thinnest oxide layer (about 2 nm native oxide). Two data sets from 0.5 to 3.0 eV and from 0.76 to 6.6 eV taken on the same day,

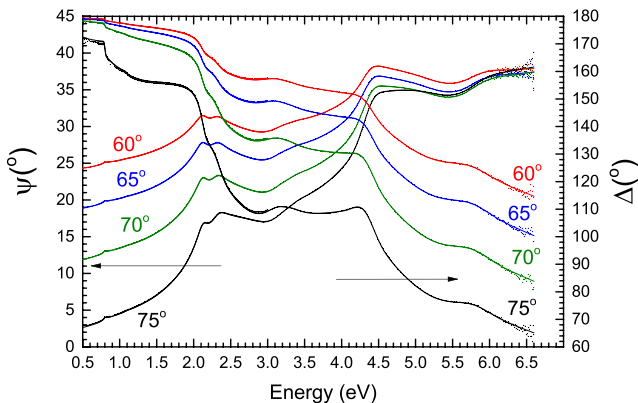


Fig. 3. (Color online) Ellipsometric angles  $\psi$  and  $\Delta$  (symbols) at four angles of incidence (60°, 65°, 70°, 75°) for a Ge wafer with native oxide, after the standard clean described in Sec. II. Two data sets from 0.5 to 3.0 eV and from 0.76 to 6.6 eV were merged. Lines: Data calculated from our model.

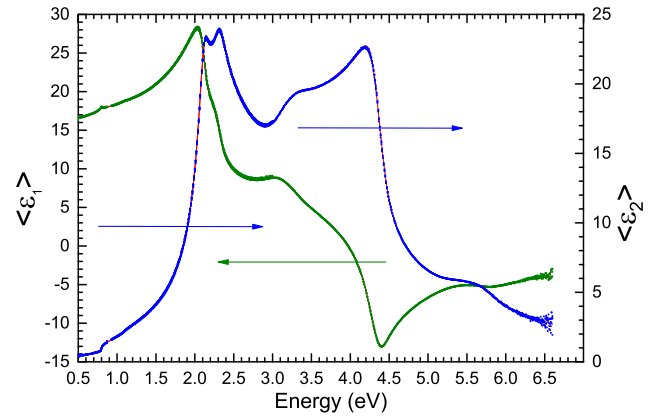


Fig. 4. (Color online) Same data as in Fig. 3 for four angles of incidence, but displayed as a complex pseudodielectric function  $\langle \epsilon \rangle$  (symbols). Data from our model are shown in red.

but under slightly different conditions, were merged in these figures. The differences between the two data sets are no more than 2% of  $\langle \epsilon \rangle$ . Most likely, these differences are due to the slight nonuniformity across the wafer surface or due to changes in surface conditions between the measurements. The depolarization for this sample is below 0.4% (except at the extreme ends of the spectral range due to noise) and peaks near 3.5 eV. There is no sign of depolarization due to backside reflections below the indirect band gap<sup>18</sup> ( $E_i=0.66$  eV).

The ellipsometric angle  $\psi$  is largest for  $\phi_0=60^\circ$  and decreases toward larger incidence angles (see Fig. 3).  $\psi$  becomes zero at the Brewster angle (76° for Ge at 2.5  $\mu\text{m}$ ).  $\psi$  increases gradually toward larger photon energies. The  $E_1$ ,  $E_1 + \Delta_1$ ,  $E'_0$ ,  $E_2$ , and  $E'_1$  critical points<sup>25</sup> are clearly visible.  $\Delta$  is near 180° in the IR and drops toward larger photon energies, as the absorption increases. There is a sharp drop near the direct gap  $E_0=0.8$  eV and additional drops at critical points with higher energies.  $\Delta$  also decreases with increasing  $\phi_0$ .

Below the direct gap,  $\Delta$  should be 180° in the absence of a surface layer, because the absorption nearly vanishes. Instead,  $\Delta \approx 170^\circ$  for  $\phi_0=75^\circ$  below 0.8 eV. For both Ge and GeO<sub>2</sub>, the refractive index at 2.5  $\mu\text{m}$  (in the transparent region) is fairly well established as 4.07 (Ge) and 1.57 (GeO<sub>2</sub>), respectively.<sup>9,19,52,53</sup> Therefore, we are able to calculate that the native oxide thickness for this sample must be about 23 Å. This native oxide thickness is consistent with our peak value of  $\langle \epsilon_2 \rangle = 22.6$  near 4.2 eV (see Fig. 4), considerably below the literature peak values<sup>24,26</sup> of 31–32 for bare Ge. We therefore fix the native oxide thickness at 23 Å for our initial fits of sample 1.

Figures 5, 6, and 7 show the ellipsometric angles and depolarization spectra for Ge wafers with thermally grown oxides of 34, 89, and 136 nm thickness. For the 34-nm sample,  $\psi$  shows a strong interference fringe near 4.8 eV, while the 89 nm sample shows two interference fringes at 2.5 and 6.0 eV. The thickest (136 nm) sample shows three interference fringes. At the same energies as the  $\psi$  fringes, we also see maxima in the depolarization, which can become quite strong (up to 40%). We model the depolarization with a

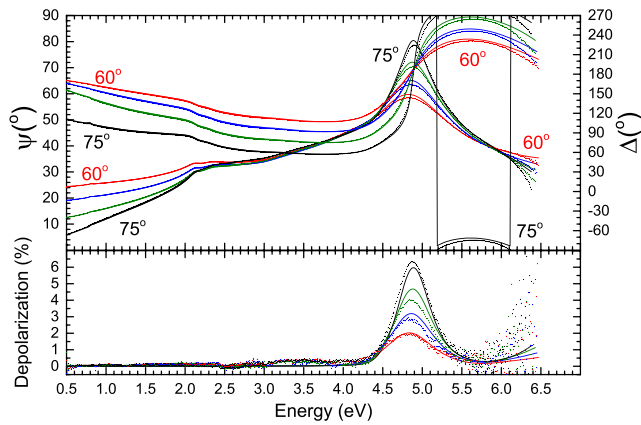


Fig. 5. (Color online) Ellipsometric angles ( $\psi$ ,  $\Delta$ ) and depolarization (symbols) for 34 nm  $\text{GeO}_2$  on Ge. Our model with a uniform oxide (lines) is nearly indistinguishable from the experimental data.

constant monochromator bandwidth of 4 nm and by selecting a thickness nonuniformity (see Table I) to match the magnitude of the largest depolarization peak in the UV.<sup>54</sup> Small lateral variations of the refractive index have the same effect as thickness nonuniformity.

Even at 6.1 eV, the  $\psi$  interference fringes are still quite strong, indicating that the absorption coefficient of  $\text{GeO}_2$  is still small at this energy. The magnitude of the  $\psi$  fringes is significantly influenced by depolarization. For example, for the same absorption coefficient ( $3 \times 10^4 \text{ cm}^{-1}$  at 6.1 eV), the peak value of  $\psi$  would be  $76^\circ$  for an ideal situation (without depolarization), but this peak is reduced to  $63^\circ$ – $65^\circ$  under nonideal (depolarizing) conditions for our films and experimental setup. Depolarizing effects therefore make it difficult to place an exact value on the absorption coefficient of  $\text{GeO}_2$ .

We are finally ready to start the fit, using the Tauc-Lorentz parameters fitted to the  $\text{GeO}_2$  optical constants<sup>33,52</sup> and parametric oscillator parameters for Ge from the *wvase32* software as starting values. The shape parameters for the  $E_0$ ,  $E_0 + \Delta_0$ ,  $E_1$ , and  $E_1 + \Delta_1$  critical points were fixed at the same values as for GaAs. We also fixed  $\Delta_0 = 0.297 \text{ eV}$  and the broadenings for  $E_0$  (10 meV) and  $E_0 + \Delta_0$  (20 meV) based on historical transmission measurements.<sup>55</sup>

The material parameters obtained from our best model are given in Tables S1 and S2 as supplementary material.<sup>56</sup> The

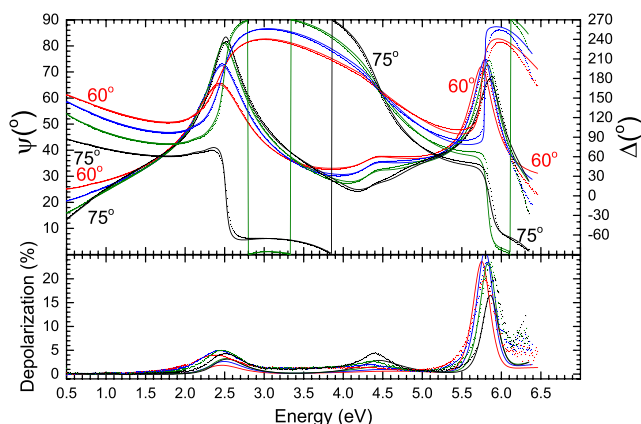


Fig. 6. (Color online) As Fig. 5, but for a Ge wafer with 89 nm  $\text{GeO}_2$ .

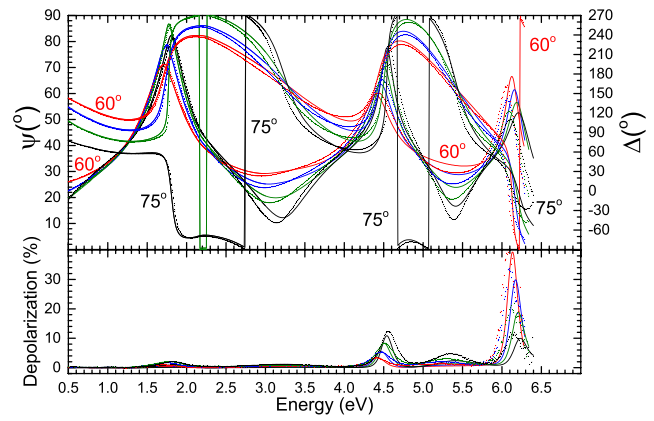


Fig. 7. (Color online) As Fig. 5, but for a Ge wafer with 136 nm  $\text{GeO}_2$ . The uniform layer model (lines) matches the maxima of  $\psi$ , but not the minima. This is a clear indication for a gradient in the refractive index of the  $\text{GeO}_2$  film.

dielectric functions for Ge and  $\text{GeO}_2$  are shown in Figs. 8 and 9 and also tabulated<sup>56</sup> in Tables S3 and S4. The MSE including all five samples in Table I was found to be 14. This means that the average deviation between data and model is about 14 times the experimental errors. Half of the MSE is from the thickest oxide layer as will be discussed later. Our model gives a near-perfect fit ( $\text{MSE} = 0.9$ ) for the Ge substrate with native oxide, but deviations are larger for the thicker oxides. The MSE is just slightly larger ( $\text{MSE} = 18$ ) for a nonabsorbing model for  $\text{GeO}_2$  using two UV poles. We suspect that the largest sources of deviation for the thicker oxide samples are the depolarization and errors in the ellipsometric angles (especially in the UV) due to thickness variations across the samples.

To estimate the accuracy of the  $\text{GeO}_2$  optical constants shown in Fig. 9, we proceed as follows: The black lines in Fig. 10 show the best fit to all samples with a uniform Tauc-Lorentz layer for the  $\text{GeO}_2$  oxide. This fit also determines the thicknesses of all oxides (see Table I). Next, we only fit the 89 nm oxide with an uncorrelated all-wavelength inversion of the ellipsometric angles at fixed thickness, where Kramers–Kronig consistence is not enforced. (This is also known as a point-by-point fit.) The results of this fit are

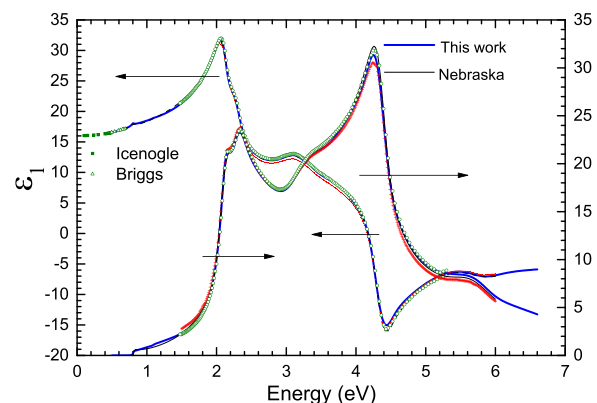


Fig. 8. (Color online) Complex dielectric function for Ge from a fit to our ellipsometry results in comparison with literature data (Refs. 9, 19, 24, 26, and 42).

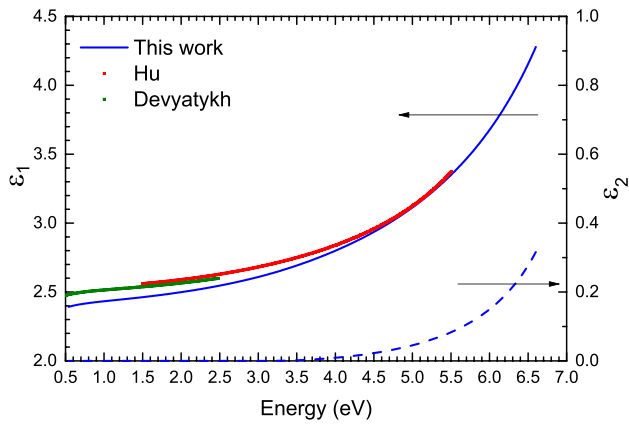


FIG. 9. (Color online) Complex dielectric function for  $\text{GeO}_2$  from the uniform layer fit to our ellipsometry results in comparison with literature data (Refs. 33 and 52).

shown by symbols in Fig. 10. We then perform the same fit for another sample with 136 nm thickness and also show the results by symbols. We can see that the differences between the Tauc-Lorentz fit to all samples (assuming uniform identical oxide layers) and the single-sample point-by-point fits are quite large (up to 10% for  $\epsilon_1$ ). Furthermore, we see oscillations in the data, which are probably artifacts due to incomplete removal of interference fringes. Values of  $\epsilon_2 < 0.1$  are probably not reliable, but it appears that there is some absorption in the oxide above 6 eV. It has been reported<sup>57</sup> that the absorption coefficient of  $\text{GeO}_2$  depends on the details of preparation. Therefore, it is possible that poor agreement between data and model in the deep UV is due to sample-to-sample variations, which we have ignored in our model.

## V. RESULTS FOR $\text{GeO}_2$ ON Ge WITH NONUNIFORM LAYER FITS

Since the quality of our fit with a three-phase (ambient-film-substrate) model is only moderate (MSE = 14), we

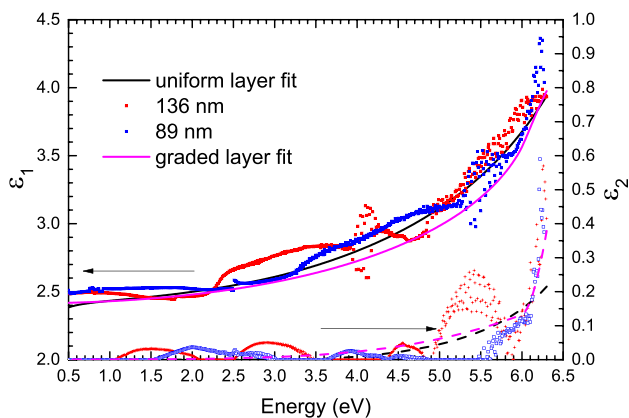


FIG. 10. (Color online) To estimate the accuracy of the optical constants for  $\text{GeO}_2$ , we plot the dielectric function obtained from various methods: From a Tauc-Lorentz fit to all data assuming uniform oxide density, from fits of single samples (89 and 136 nm thickness) with a uniform density, and a two-oscillator fit (Tauc-Lorentz and Gaussian) to all data allowing a density gradient for the thicker oxides.

discuss how the fit might be improved by adding more complexity to our model. We focus on the UV spectral region, where the discrepancy between data and model is largest. (For sample 1, the native oxide, the differences between the measured ellipsometric angles and the model are much less than  $1^\circ$ . The differences reach several degrees or even more for thicker oxides, especially in the UV.) First, we note that adding additional oscillators in the UV spectral region for  $\text{GeO}_2$  (beyond the Tauc-Lorentz oscillator and poles at 11 and 0.05 eV) does not reduce the overall MSE.

Next, we allow the density of the thickest oxides to vary between the bottom and top by adding a variable-density layer on top (effective medium layer with variable thickness and variable void fraction). This reduces the MSE to 8.3 and somewhat improves the fit in the UV for the thicker oxides. The void fraction in this layer is quite low (near 20%) and the thickness is large, several tens of nanometers. This model would also account for surface roughness as a special case (with a 50% void fraction), which does not appear to be a major factor due to the low void fraction resulting from the fit. Similar results can be obtained by describing the oxide as an effective medium, where the void fraction follows a power law with a large exponent (about 5) and reaches about 30% near the surface. Finally, our best model (MSE = 6.9) adds an additional Gaussian oscillator for  $\text{GeO}_2$  in the UV, which leads to a kink in the absorption, as shown in Fig. 10.

As a generalization of this effective-medium-approximation (EMA) model, we can also describe the oxides with a graded-layer model, where the complex refractive index depends on thickness through a power law with a variable exponent. The refractive index in such oxide models is typically about 20% lower at the surface than at the substrate/oxide interface and the exponent is quite high (indicating that the low-density region is confined to the top 20% of the film).

We also added an interfacial layer with variable thickness (kept the same for all samples), which consists of a 50/50 mixture of the bulk and film optical constants described within the Bruggeman EMA. The rationale for this model is that some electrons in the bulk Ge might leak out into the oxide (have a finite probability to be located in the  $\text{GeO}_2$  barrier). It has also been shown theoretically<sup>58</sup> for the Si/ $\text{SiO}_2$  interface that the first 7–10 Å of the oxide have a different structure and density than thick oxides. Using this “intermix” model,<sup>8</sup> which assumes a higher electron density near the interface than in a thick oxide, did not improve our fits, and therefore, we discarded this possibility.

## VI. DISCUSSION

Since a three-layer (ambient-oxide-substrate) model with uniform  $\text{GeO}_2$  layers gives good agreement with our ellipsometry data and cannot be improved much by introducing more complexity, we consider the results from our uniform three-layer fit the final results from this work. The results for the complex dielectric function, complex refractive index, absorption coefficient, and normal-incidence reflectance for Ge and  $\text{GeO}_2$  as a function of photon energy and wavelength

are given in Tables S3 and S4 of the supplementary material.<sup>56</sup>

The complex dielectric function of Ge from our fit together with literature results<sup>24,26</sup> and an unpublished data set<sup>42</sup> are shown in Fig. 8. Our  $\epsilon_2$  maximum of 31.3 at 4.25 eV is between the results of Refs. 24 and 26 and slightly lower than the unpublished Nebraska result<sup>42</sup> of  $\epsilon_2 = 32.3$ . Since we determined the oxide thickness for our thinnest sample (native oxide) using the Jellison–Sales method<sup>30</sup> with measurements below the Ge band gap, we believe that our results are highly accurate. At 0.5 eV, below the band gap, our refractive index  $n = 4.07$  is identical to minimum-deviation prism results.<sup>9,19</sup> The maxima and minima of our spectra related to critical points and interband transitions<sup>25</sup> have been discussed elsewhere.<sup>59</sup>

Figure 9 shows the dielectric function for GeO<sub>2</sub> from our fit in comparison with prior data.<sup>33,52</sup> The results for thermal oxides produced by Hu *et al.*<sup>33</sup> cover the energy range from 1.5 to 5.5 eV, while Devyatkh *et al.*<sup>52</sup> measured bulk crystals from 0.5 to 2.5 eV using the minimum-deviation prism method.

Our value of  $\epsilon_1$  at 0.5 eV for the oxide film equals 2.4 (corresponding to  $n = 1.55$ ), which is about 4% lower than prior results.<sup>33,52</sup> Our values do not depend much on the details of our Tauc-Lorentz model (such as the strength of the IR pole, the Tauc gap, or including a density gradient). Therefore, it is possible that our GeO<sub>2</sub> oxides indeed have a lower density (resulting in a lower refractive index) than films and crystals produced by others, perhaps related to our fast high-pressure oxidation conditions (see Fig. 1). For the Si/SiO<sub>2</sub> system, it is known that oxides with lower density have a lower refractive index.<sup>60–63</sup> Variations of the index of a silicate glass by 5%–10% are common (even without adding heavy metals to increase the index). On the other hand, Fig. 10 also demonstrates that the accuracy of our GeO<sub>2</sub> refractive index measurement is only about 5%, because an oscillator fit may yield a different result than a direct point-by-point inversion. Pajasova<sup>53</sup> provided accurate measurements of the refractive index  $n$  for bulk glassy GeO<sub>2</sub> in the transparent region from 0.4 to 2.5  $\mu\text{m}$  using the minimum-deviation prism measurements. She found that  $n$  decreases from 1.57 at 1  $\mu\text{m}$  to 1.56 at 2.5  $\mu\text{m}$  ( $\epsilon_1 = 2.43$ ), quite similar to our values.

Pajasova's<sup>53</sup> results for  $\epsilon_2$  of GeO<sub>2</sub> are less accurate, because they were obtained from Kramers-Kronig transformation of reflectance data, but they clearly indicate strong absorption peaks at 6.6 and 10.7 eV, outside of our spectral range. From measurements on rf-sputtered GeO<sub>2</sub> films with 0.77–6  $\mu\text{m}$  thickness,<sup>41</sup> the onset of strong absorption was found to be about 5.95 eV. Below the main band gap, there is an absorption peak with a magnitude of about  $200\text{ cm}^{-1}$  centered at 5.06 eV, which was found in bulk crystals<sup>57</sup> as well as in thin films.<sup>41</sup> This peak depends on preparation conditions and disappears after annealing at high temperatures of bulk specimens or films on fused silica.<sup>41</sup> This below-gap absorption has been attributed to oxygen vacancies,<sup>57</sup> which are also expected in our thermal oxides due to oxide decomposition.<sup>36</sup> In our absorption coefficient data

derived from  $\epsilon$  for GeO<sub>2</sub>, we determine  $\alpha = 2 \times 10^4\text{ cm}^{-1}$  (the threshold of our sensitivity, compare Fig. 10) at 6 eV, considerably larger than  $\alpha = 0.5 \times 10^4\text{ cm}^{-1}$  found by transmission measurements on sputtered films.<sup>41</sup> It is common for spectroscopic ellipsometry measurements to overestimate small absorption coefficients.<sup>20,21</sup>

## VII. SUMMARY

We developed a hybrid dry-wet preclean for thermal oxidation of Ge and produced thermal oxides on Ge at 550 °C and 270 kPa O<sub>2</sub> pressure, with oxide thicknesses ranging from 34 to 136 nm and oxidation times up to 10 h. Multisample ellipsometry analysis of these oxides determined the dielectric functions of Ge and GeO<sub>2</sub> from 0.5 to 6.6 eV. We carefully discuss the accuracy of our results and compare with prior data.

## ACKNOWLEDGMENTS

This work was supported by the Air Force Office of Scientific Research (FA9550-13-1-0022) and by the Army Research Office (W911NF-14-1-0072). Support during 2016 was provided by the National Science Foundation (DMR-1505172). J.M.M. and A.A.M. acknowledge support from the New Mexico Alliance for Minority Participation (NM-AMP).

<sup>1</sup>A. Diebold, *Handbook of Silicon Semiconductor Metrology* (Marcel Dekker, New York, 2001).

<sup>2</sup>T. Yoshizawa, *Handbook of Optical Metrology: Principles and Applications* (CRC, Boca Raton, FL, 2009).

<sup>3</sup>S. Zollner, *Ellipsometry at the Nanoscale*, edited by M. Losurdo and K. Hingerl (Springer, Berlin, 2013), pp. 607–627.

<sup>4</sup>H. G. Tompkins and W. A. McGahan, *Spectroscopic Ellipsometry and Reflectometry: A User's Guide* (Wiley, New York, 1999).

<sup>5</sup>H. Fujiwara, *Spectroscopic Ellipsometry: Principles and Applications* (Wiley, Chichester, 2007).

<sup>6</sup>H. G. Tompkins and E. A. Irene, *Handbook of Ellipsometry* (Springer, Heidelberg, 2005).

<sup>7</sup>H. G. Tompkins and J. N. Hilfiker, *Spectroscopic Ellipsometry: Practical Application to Thin Film Characterization* (Momentum, New York, 2016).

<sup>8</sup>C. M. Herzinger, B. Johs, W. A. McGahan, J. A. Woollam, and W. Paulson, *J. Appl. Phys.* **83**, 3323 (1998).

<sup>9</sup>R. F. Potter, *Handbook of Optical Constants of Solids*, edited by E. D. Palik (Academic, San Diego, CA, 1998), pp. 462–475.

<sup>10</sup>S. Adachi, *The Handbook on Optical Constants of Semiconductors* (World Scientific, Singapore, 2012).

<sup>11</sup>M. Fox, *Optical Properties of Solids*, 2nd ed. (Oxford University, Oxford, 2010).

<sup>12</sup>M. L. Cohen and J. R. Chelikowsky, *Electronic Structure and Optical Properties of Semiconductors* (Springer, Berlin, 1988).

<sup>13</sup>P. Y. Yu and M. Cardona, *Fundamentals of Semiconductors: Physics and Materials Properties*, 4th ed. (Springer, Berlin, 2010).

<sup>14</sup>D. G. Seiler, S. Zollner, A. C. Diebold, and P. M. Amirtharaj, *Handbook of Optics*, edited by M. Bass, 3rd ed. (McGraw-Hill, New York, 2010), Vol. IV, Chap. 5, pp. 5.1–96.

<sup>15</sup>W. G. Spitzer, *Semicond. Semimetals* **3**, 17 (1967).

<sup>16</sup>R. J. Collins and H. Y. Fan, *Phys. Rev.* **93**, 674 (1954).

<sup>17</sup>W. C. Dash and R. Newman, *Phys. Rev.* **99**, 1151 (1955).

<sup>18</sup>G. G. Macfarlane, T. P. McLean, J. E. Quarrington, and V. Roberts, *Phys. Rev.* **108**, 1377 (1957); *J. Phys. Chem. Solids* **8**, 388 (1959).

<sup>19</sup>H. W. Icenogle, B. C. Platt, and W. L. Wolfe, *Appl. Opt.* **15**, 2348 (1976).

<sup>20</sup>T. N. Nunley, T. I. Willett-Gies, J. A. Cooke, F. S. Manciu, P. Marsik, C. Bernhard, and S. Zollner, *J. Vac. Sci. Technol. A* **34**, 051507 (2016).

- <sup>21</sup>A. Ghosh, C. M. Nelson, L. S. Abdallah, and S. Zollner, *J. Vac. Sci. Technol., A* **33**, 061203 (2015).
- <sup>22</sup>M. Cardona and G. Harbeke, *J. Appl. Phys.* **34**, 813 (1963).
- <sup>23</sup>H. R. Philipp and E. A. Taft, *Phys. Rev.* **113**, 1002 (1959).
- <sup>24</sup>D. E. Aspnes and A. A. Studna, *Phys. Rev. B* **27**, 985 (1983).
- <sup>25</sup>L. Viña, S. Logothetidis, and M. Cardona, *Phys. Rev. B* **30**, 1979 (1984).
- <sup>26</sup>G. E. Jellison, *Opt. Mater.* **1**, 151 (1992).
- <sup>27</sup>M. K. Kelly, S. Zollner, and M. Cardona, *Surf. Sci.* **285**, 282 (1993).
- <sup>28</sup>D. E. Aspnes and A. A. Studna, *Surf. Sci.* **96**, 294 (1980).
- <sup>29</sup>K. A. Bell, L. Mantese, U. Rossow, and D. E. Aspnes, *Thin Solid Films* **313–314**, 161 (1998).
- <sup>30</sup>G. E. Jellison and B. C. Sales, *Appl. Opt.* **30**, 4310 (1991).
- <sup>31</sup>B. E. Deal and A. S. Grove, *J. Appl. Phys.* **36**, 3770 (1965).
- <sup>32</sup>G. Hellings *et al.*, *IEEE Electron Devices Lett.* **30**, 88 (2009).
- <sup>33</sup>Y. Z. Hu, J.-Th. Zettler, S. Chongsawangvirod, Y. Q. Wang, and E. A. Irene, *Appl. Phys. Lett.* **61**, 1098 (1992).
- <sup>34</sup>P. Ponath, A. B. Posadas, R. C. Hatch, and A. A. Demkov, *J. Vac. Sci. Technol., B* **31**, 031201 (2013).
- <sup>35</sup>H. Adhikari, P. C. McIntyre, S. Sun, P. Pianetta, and C. E. D. Chidsey, *Appl. Phys. Lett.* **87**, 263109 (2005).
- <sup>36</sup>S. R. M. da Silva, G. K. Rolim, G. V. Soares, I. J. R. Baumvol, C. Krug, L. Miotti, F. L. Freire, M. E. H. M. da Costa, and C. Radtke, *Appl. Phys. Lett.* **100**, 191907 (2012).
- <sup>37</sup>K. Kita, S. Suzuki, H. Nomura, T. Takahashi, T. Nishimura, and A. Toriumi, *Jpn. J. Appl. Phys., Part 1* **47**, 2349 (2008).
- <sup>38</sup>H. Matsubara, T. Sasada, M. Takenaka, and S. Takagi, *Appl. Phys. Lett.* **93**, 032104 (2008).
- <sup>39</sup>J. T. Law and P. S. Meigs, *J. Electrochem. Soc.* **104**, 154 (1957).
- <sup>40</sup>R. B. Bernstein and D. Cubicciotti, *J. Am. Chem. Soc.* **73**, 4112 (1951).
- <sup>41</sup>P. Bohač, L. Jastrabik, D. Chvostova, and V. Zelezny, *Vacuum* **41**, 1466 (1990).
- <sup>42</sup>J.A. Woollam Co., Inc., Lincoln, NE.
- <sup>43</sup>G. E. Jellison and F. A. Modine, *Appl. Phys. Lett.* **69**, 371 (1996); **69**, 2137 (1996).
- <sup>44</sup>J. Leng, J. Opsal, H. Chu, M. Senko, and D. E. Aspnes, *J. Vac. Sci. Technol., A* **16**, 1654 (1998).
- <sup>45</sup>A. Kahan, J. W. Goodrum, R. S. Singh, and S. S. Mitra, *J. Appl. Phys.* **42**, 4444 (1971).
- <sup>46</sup>E. R. Lippincott, A. Van Valkenburg, C. E. Weir, and E. N. Bunting, *J. Res. Natl. Bur. Stand.* **61**, 61 (1958).
- <sup>47</sup>M. Hass, *J. Phys. Chem. Solids* **31** 415 (1970).
- <sup>48</sup>M. Erman, J. B. Theeten, N. Vodjdani, and Y. Demay, *J. Vac. Sci. Technol., B* **1**, 328 (1983).
- <sup>49</sup>D. E. Aspnes, *Handbook on Semiconductors: Optical Properties of Solids*, edited by M. Balkanski (North-Holland, Amsterdam, 1980), Vol. 2, p. 109.
- <sup>50</sup>C. C. Kim, J. W. Garland, H. Abad, and P. M. Raccach, *Phys. Rev. B* **45**, 11749 (1992).
- <sup>51</sup>C. M. Herzinger and B. D. Johs, U.S. patent 5,796,983 (18 August 1998).
- <sup>52</sup>G. G. Devyatikh *et al.*, *Sov. J. Quantum Electron.* **10**, 900 (1980).
- <sup>53</sup>L. Pajasova, *Czech. J. Phys. B* **19**, 1265 (1969).
- <sup>54</sup>G. E. Jellison and J. W. McCamy, *Appl. Phys. Lett.* **61**, 512 (1992).
- <sup>55</sup>T. P. McLean and E. G. S. Paige, *Report of the International Conference on the Physics of Semiconductors*, edited by A. C. Stickland (Institute of Physics, London, 1962), p. 450.
- <sup>56</sup>See supplementary material at <http://dx.doi.org/10.1116/1.4963075> for a listing of the oscillator parameters for Ge and GeO<sub>2</sub> and for tables of the optical constants of these materials.
- <sup>57</sup>J. M. Jackson, M. E. Wells, G. Kordas, D. L. Kinser, R. A. Weeks, and R. H. Magruder, *J. Appl. Phys.* **58**, 2308 (1985).
- <sup>58</sup>A. A. Demkov and O. F. Sankey, *Phys. Rev. Lett.* **83**, 2038 (1999).
- <sup>59</sup>N. S. Fernando *et al.*, “Temperature dependence of the interband critical points of bulk Ge and strained Ge on Si,” *Appl. Surf. Sci.* (accepted).
- <sup>60</sup>W. A. Pliskin, *J. Vac. Sci. Technol.* **14**, 1064 (1977).
- <sup>61</sup>K. Taniguchi, M. Tanaka, C. Hamaguchi, and K. Imai, *J. Appl. Phys.* **67**, 2195 (1990).
- <sup>62</sup>N. Kitamura, K. Fukumi, J. Nishii, and N. Ohno, *J. Appl. Phys.* **101**, 123533 (2007).
- <sup>63</sup>W. Rzdokiewicz and A. Panas, *Acta Phys. Pol., A* **116**, S-92 (2009).